Biosensors and Bioelectronics 116 (2018) 116–122

Contents lists available at ScienceDirect

Biosensors and Bioelectronics

journal homepage: www.elsevier.com/locate/bios

Gold nanorod embedded novel 3D graphene nanocomposite for selective bio-capture in rapid detection of *Mycobacterium tuberculosis*

Veeradasan Perumal[a,g], Mohamed Shuaib Mohamed Saheed[a,b], Norani Muti Mohamed[a,b,*], Mohamed Salleh Mohamed Saheed[a,b], Satisvar Sundera Murthe[a,b], Subash C.B. Gopinath[c,d], Jian-Ming Chiu[e,f]

[a] Centre of Innovative Nanostructures and Nanodevices (COINN), Universiti Teknologi PETRONAS, 32610 Seri Iskandar, Perak Darul Ridzuan, Malaysia
[b] Department of Fundamental and Applied Sciences, Universiti Teknologi PETRONAS, 32610 Seri Iskandar, Perak Darul Ridzuan, Malaysia
[c] Institute of Nano Electronic Engineering, Universiti Malaysia Perlis, 01000 Kangar, Perlis, Malaysia
[d] School of Bioprocess Engineering, Universiti Malaysia Perlis, 02600 Arau, Perlis, Malaysia
[e] Institute of Atomic and Molecular Sciences, Academia Sinica, Taipei 10617, Taiwan
[f] Department of Chemical Engineering, National Taiwan University of Science and Technology, Taipei 10607, Taiwan
[g] Mechanical Engineering Department, Universiti Teknologi PETRONAS, 32610 Seri Iskandar, Perak Darul Ridzuan, Malaysia

ARTICLE INFO

Keywords:
3D graphene
Gold nanorod
Nanocomposite
Bio-capture
Tuberculosis
Impedimetric

ABSTRACT

Tuberculosis (TB) is a chronic and infectious airborne disease which requires a diagnosing system with high sensitivity and specificity. However, the traditional gold standard method for TB detection remains unreliable with low specificity and sensitivity. Nanostructured composite materials coupled with impedimetric sensing utilised in this study offered a feasible solution. Herein, novel gold (Au) nanorods were synthesized on 3D graphene grown by chemical vapour deposition. The irregularly spaced and rippled morphology of 3D graphene provided a path for Au nanoparticles to self-assemble and form rod-like structures on the surface of the 3D graphene. The formation of Au nanorods were showcased through scanning electron microscopy which revealed the evolution of Au nanoparticle into Au islets. Eventually, it formed nanorods possessing lengths of ~ 150 nm and diameters of ~ 30 nm. The X-ray diffractogram displayed appropriate peaks suitable to defect-free and high crystalline graphene with face centered cubic Au. The strong optical interrelation between Au nanorod and 3D graphene was elucidated by Raman spectroscopy analysis. Furthermore, the anchored Au nanorods on 3D graphene nanocomposite enables feasible bio-capturing on the exposed Au surface on defect free graphene. The impedimetric sensing of DNA sequence from TB on 3D graphene/Au nanocomposite revealed a remarkable wide detection linear range from 10 fM to 0.1 μM, displays the capability of detecting femtomolar DNA concentration. Overall, the novel 3D graphene/Au nanocomposite demonstrated here offers high-performance bio-sensing and opens a new avenue for TB detection.

1. Introduction

Tuberculosis (TB) has been listed as one of the top ten causes of death worldwide in 2016 and it has been estimated that nearly 10.4 million people are infected with TB and over 1.8 million TB patients have succumbed to the illness (Global Tuberculosis Report, 2017). Currently, myriad of TB infections go undetected at the onset of the infection and detection at late stages increases the risk of transmitting TB to others tremendously. As such, it is crucial to possess a high-quality diagnostics system for early, rapid and precise detection of TB and to identify drug-resistance strains. Tuberculosis Skin Test (TST), Tuberculosis Blood Test (TBT) and Nucleic Acid Amplification (NAA) are the most common clinical detection methods which have been used by many clinical professionals as they are recommended by WHO. However, the specificity of these tests are relatively low, possess limited distinguishing ability, the measurement takes a long time to obtain a valid result all the while being prone to performance errors which may lead to false results (Srivastava et al., 2016). This necessitates a rapid, cost-effective and sensitive biosensor capable of detecting TB in patient samples such as sputum, blood and urine (Shojaei et al., 2014).

Advancements in nanotechnology over the past decades have bestowed us the tools and materials for alternate method for TB detection (Gopinath et al., 2016). The successful isolation of mono-layered graphene by Geim and Novoselov has opened a wide range of

* Corresponding author.
E-mail addresses: veeradasan.perumal@utp.edu.my (V. Perumal), noranimuti_mohamed@utp.edu.my (N.M. Mohamed).

https://doi.org/10.1016/j.bios.2018.05.042
Received 1 March 2018; Received in revised form 8 May 2018; Accepted 24 May 2018
Available online 25 May 2018
0956-5663/

opportunities enabling the interaction of chemical and biological elements at the nanoscale (Saheed et al., 2017). Special focus has been given to two-dimensional graphene materials for biological and chemical sensing due to their distinct chemical, physical, optical and electrical characteristics. However, top-down synthesis of graphene via mechanical and chemical exfoliation has major drawbacks such as limited specific surface area due to the strong π-π interaction between graphene sheets (Georgakilas et al., 2012). In addition to that, mechanical and chemical exfoliation leads to large defects and chemical group attachments to the graphene structure which results in significant deterioration of graphene properties (Qiu et al., 2017).

Recent breakthroughs in bottom-up fabrication techniques, primarily via self-assembly of materials using chemical vapour deposition (CVD) has enabled the development of microporous three-dimensional (3D) graphene (Chen et al., 2011). The synthesis of nanocomposites through a bottom-up process, where small units are assembled together to form complex nanostructures will pave the path for the construction of highly sensitive and selective biosensors (Perumal et al., 2015b). The unique interconnected network structure of 3D graphene possesses large specific surface area, strong mechanical strength and fast electron transport kinetic (Shi et al., 2017). The 3D graphene microporous structure also exhibits excellent physical, mechanical and electrical properties in addition to the intrinsic properties of 2D graphene (Fang et al., 2015; Gao and Duan, 2015). It also shows great promise for many applications such as catalytic activity, energy storage, sensing and biological applications (Yan et al., 2017).

Furthermore, noble metal nanoparticles with excellent catalytic activities have been widely employed for diverse applications by taking advantage of their superior optoelectronic and electrical properties (Perumal et al., 2015a). Moreover, the addition of noble metals to carbon materials can lead to improved conductivity, mechanical stability and generate versatile nanocomposites (Al-ani et al., 2017; Sundaram et al., 2011). Novel nanostructures using gold (Au) can be synthesized on 3D graphene substrate to fabricate nanobiosensors with large active surface area and high charge transfer properties. Au nanostructures are particularly promising and bio-compatible for DNA sensing due to its ability to enhance biomolecular attachment and further provide a passage for anchoring thiolated/sulfydryl DNA. In spite of that, there has not been much focus on Au nanostructures anchoring on 3D graphene grown by chemical vapour deposition (CVD). In this research work, we report novel Au nanorod formation through continuous sputtering on the surface of 3D graphene. Furthermore, the surface morphology and structural properties of the novel Au nanorods embedded 3D graphene were investigated for the development of TB analytical devices. The synthesized Au nanorods on 3D graphene laid the groundwork for the development of highly sensitive, selective and flexible sensing platform which uncovered untrodden paths for biosensor development.

2. Methods

2.1. Materials and reagents

A monolithic 3D graphene was synthesized using a microporous nickel foam as a sacrificial template (300 × 300 mm, thickness 1.6 mm, bulk density 0.45 g/cm^3; Sigma Aldrich, USA). First, acetone (J.T. Baker, USA), isopropanol (IPA, J.T. Baker, USA) and deionized (DI) water were used to clean the nickel foam prior to subjecting the nickel template to chemical vapour deposition. Then, poly-methyl methacrylate (PMMA, Sigma Aldrich, USA) with a concentration of 1.4% was dissolved in anisole (Sigma Aldrich, USA) to facilitate the removal of nickel template by functioning as binder. The nickel sacrificial template was then etched using iron (III) chloride ($FeCl_3$; Merck KGaA, USA) and hydrochloric acid (HCl; 32%; J.T. Baker, USA).

The oligonucleotides were purchased from First BASE laboratories Sdn. Bhd (Selangor, Malaysia). The 28-mers oligonucleotide sequences used in this work are elucidated below:

Thiolated probe DNA (p-DNA) – 5′-SH-(CH2)3-GAG TCT CCG GAC ATG CCG GGG TTC A-3′; complementary target DNA (t-DNA): 5′-T GAA CCC CGG CAT GTC CGG AGA CTC-3′; non-complementary target DNA (nc-DNA): 5′-G TGC ATA GAT AAA TCG TTT CAG ACT-3′; one-base mismatching target DNA (m-DNA): 5′-T GAA CCC CGG CAT GCC CGG AGA CTC-3′; three-base mismatching target DNA (tm-DNA): 5′-T GGA CCC CGG CAT GCC CGG AGA ATC-3′;

The single-strand thiolated probe DNA (p-DNA) was designed from IS6110 genes that were obtained from GenBank database. The whole genomic sequence can be found in GenBank under the accession number: AJ242908.1.

2.2. CVD growth of 3D graphene

The microporous sponge-like 3D graphene was synthesized on a porous nickel template through a CVD method reported previously (Chen et al., 2011; Saheed et al., 2017). In brief, prior to the growth process, the porous nickel form was thoroughly cleaned with acetone and vigorously rinsed with isopropanol and DI water to remove any organic impurities. The nickel foam was then loaded in a horizontal CVD quartz tube and heated to 1000 °C with a constant flow of hydrogen and argon for template activation and removal of residual oxygen species. Next, methane was introduced into the system and its subsequent decomposition led to the formation of graphene layers on the nickel template. 3D graphene was obtained on the nickel template after rapid cooling of the substrate to ambient temperature under hydrogen and argon flow. The nickel template was then etched using 1.0 M of iron (III) chloride and 0.2 M of hydrochloric acid. In order to maintain the structural integrity of the 3D graphene, PMMA was coated onto the exposed surface prior to nickel template removal. Finally, the sponge-like free standing microporous 3D graphene was obtained after complete PMMA removal using acetone at 80 °C.

2.3. Au nanorods formation on 3D graphene via sputtering

Au nanorods growth on 3D graphene was achieved via sputtering. The sputtering process and method are similar to a previous study (Perumal et al., 2015a, 2015b). The difference is that the sputtering thickness varies from 10, 15, 20 and 25 nm Au wetting layers. The detailed experimental conditions are as follows: electric current was maintained at 25 mA for 2, 3, 4 and 5 min with a vacuum pressure of Argon process level at 10^{-2} mbar. This process allowed us to obtain Au nanorods formation on 3D graphene.

2.4. Tuberculosis DNA immobilization and hybridization

The Au nanorods sputtered 3D graphene electrodes were cleaned, dried and was used to fabricate DNA biosensors for the detection of *Mycobacterium tuberculosis*. The covalent bond contact between Au nanostructured and thiolated probe DNA was established by dispensing 10 μL of 1 μM thiolated probe DNA solution in Tris-EDTA buffer for 3 h, followed by washing and rinsing of the electrode with sterile double-distilled water. Next, the target DNA with various concentrations (10 fM to 0.1 μM) was immobilized onto the electrode with a few drops of the DNA sample for hybridization analysis. The complete modification of the electrode along with immobilization and hybridization is schematically illustrated in Fig. 1a. Furthermore, mismatch, non-complementary and cross-specificity of DNA were thoroughly investigated.

2.5. Morphological, structural, optical and electrical characterization

The surface morphology of the fabricated structures were investigated using a variable pressure (VP) FESEM (Carl Zeiss SUPRA55 VP, Gemini). Electrical measurements of current to voltage (I–V) and electrochemical impedance spectroscopy were taken using HMS-3000

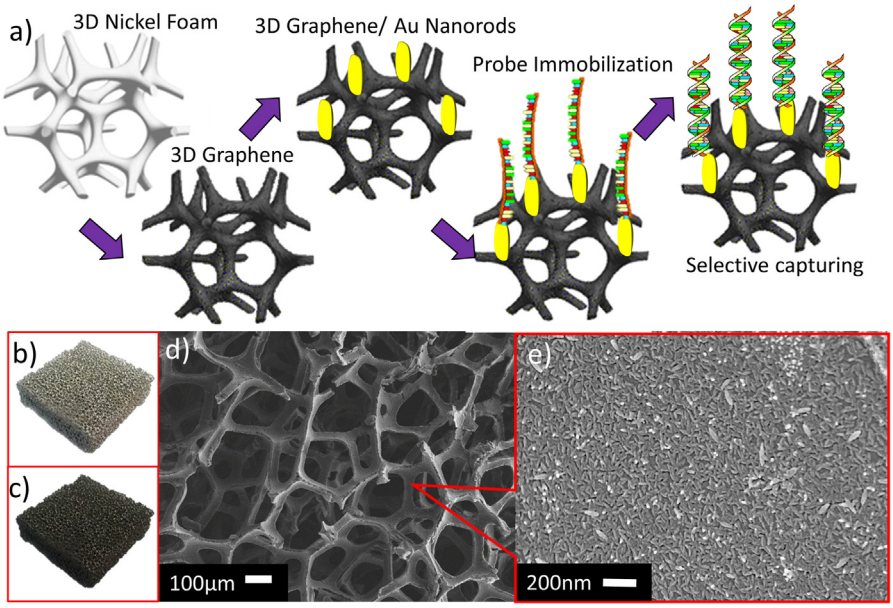

Fig. 1. (a) Schematic illustration representing the synthesis of Au nanorod embedded 3D graphene nanocomposite, immobilization and hybridization process. Nickel foam before (b) and after (c) CVD synthesis are displayed. The honey-combed 3D graphene structure, (d) with FESEM image of high magnification (e) displaying Au nanorods formation on 3D graphene.

Hall Measurement System and Autolab PGSTAT302N, respectively. Electrochemical impedance spectroscopy (EIS) measurements were taken in the frequency range of 1–100 MHz with AC amplitude of 1 V RMS. All the measurements were recorded at room temperature. Additionally, the structural properties of the 3D graphene were studied extensively using Raman spectroscopy (HORIBA Jobin Yvon HR800) and X-Ray Diffraction (Bruker D8, Bruker AXS, Inc., Madison, WI, USA).

3. Results and discussion

The development of Au nanorods on 3D graphene was discovered when the adherence of Au nanoparticles on the surface of 3D graphene via the sputtering method was being investigated. In order to study the formation of Au nanorods on 3D graphene, a plethora of studies were conducted. Au nanorods distinctly formed on 3D graphene, due to the unique morphology of 3D graphene which strengthens its overall structure as compared to Au nanoparticles which are sputtered on a silicon wafer. The smooth surface of silicon wafer does not incite the formation nanorod-like structures (Supplementary Fig. 1). The 3D graphene grown via CVD exhibits a unique irregularly spaced structure with rippled surfaces that cause the Au nanoparticles to self-assemble into rod-like structures (Supplementary Fig. 2). The morphological analysis of Au nanorods on 3D graphene which was studied using field-emission scanning electron microscopy (FESEM), clearly reveals the steps leading to the formation of Au nanorods on 3D graphene which varies as sputtering time increases (Supplementary Figs. 2 and 3). The Au nanoparticles progresses to form an islet and finally rod-like structure on 3D graphene, as the thickness of Au being sputtered increases. Furthermore, the structural analyses via X-ray diffraction and Raman spectroscopy of increasing Au sputtering are clearly illustrated in Supplementary Figs. 4 and 5, respectively. The Au nanorods and 3D graphene nanocomposite provide unprecedented high surface areas and specificity (SSA), fast electron transport, strong mechanical strength and high catalytic activity owing to the combination of 3D porous structures and the excellent intrinsic properties of Au. In lieu of that, we investigated the bio-sensing ability of the 3D graphene/Au nanorods nanocomposite to detect Mycobacterium tuberculosis (MTB) DNA from the IS6110 gene, which is a target that shows tremendous potential in diagnostic tests for tuberculosis (TB). We describe here a method to systematically study the energetics of 3D graphene/Au nanorod nanocomposite through impedimetric analysis of MTB.

3.1. Morphological study of Au nanorods formation on 3D graphene

Fig. 1(b, c) depict the images of nickel foam before and after CVD synthesis. The changes in the colour of nickel foam prior to CVD and post-CVD indicate the successful synthesis of microporous 3D graphene. The FESEM image in Fig. 2a reveals the formation of microporous sponge-like network of 3D graphene. A careful observation on higher magnification through FESEM (Fig. 2b) clearly shows that the ligament-like interconnected network structure of 3D graphene closely imitates the intrinsic structure of microporous nickel foam with a width about 70–100 µm. The synthesized microporous 3D graphene also sustains the 3D structure integrity upon removal of nickel template demonstrating excellent mechanical strength. The CVD rapid cooling in 3D graphene synthesis contributes to the difference in thermal expansion coefficients between the nickel template and graphene, in which the nickel foam retracts faster compared to graphene (Xiao et al., 2012). Hence, ripples and wrinkles at micro and nanoscale are formed on the surface of 3D graphene, which is clearly showcased in Fig. 2c. The FESEM image displayed in Fig. 2d proves Au agglomeration over the entire surface of the 3D graphene. A keen observation of the nanocomposite surface with enhanced magnification by FESEM (Fig. 2(e, f)), reveals the expanded Au nanoparticle islet yielding a rod-like structure on the 3D graphene surface. The uniformly distributed rod-like structures of Au on the surface of 3D graphene contributes to the formation of a high active surface area. This modification on the surface of 3D graphene provides an efficient path for chemisorption of thiolated probe DNA during immobilization and target DNA hybridization. Further, the comparison of FESEM image of pre and post Au nanorods self-assembly shown in Supplementary Figs. 6 and 7.

3.2. Structural analyses of 3D graphene/Au nanorods composite

The Au nanorods obtained on 3D graphene were further characterized by X-ray diffraction (XRD) to study its purity and crystallinity. Fig. 3(a, b) shows the XRD patterns of bare 3D graphene before and after the formation of rod-like Au nanostructure. The diffraction peak in Fig. 3a can be indexed to graphitic carbon structure and appears at 26.5° and 54.5° for (002) and (004) planes, respectively (JCPDS 75-1621). The sharp peak at 26.5° plane of (002) is attributed to the synthesis of defect-free and highly crystalline graphene (Sahoo et al., 2015). The diffraction peak corresponding to Au at 38.5° and 44.6° for (111) and (200) planes were matched with bulk Au JCPDS card no. 65-

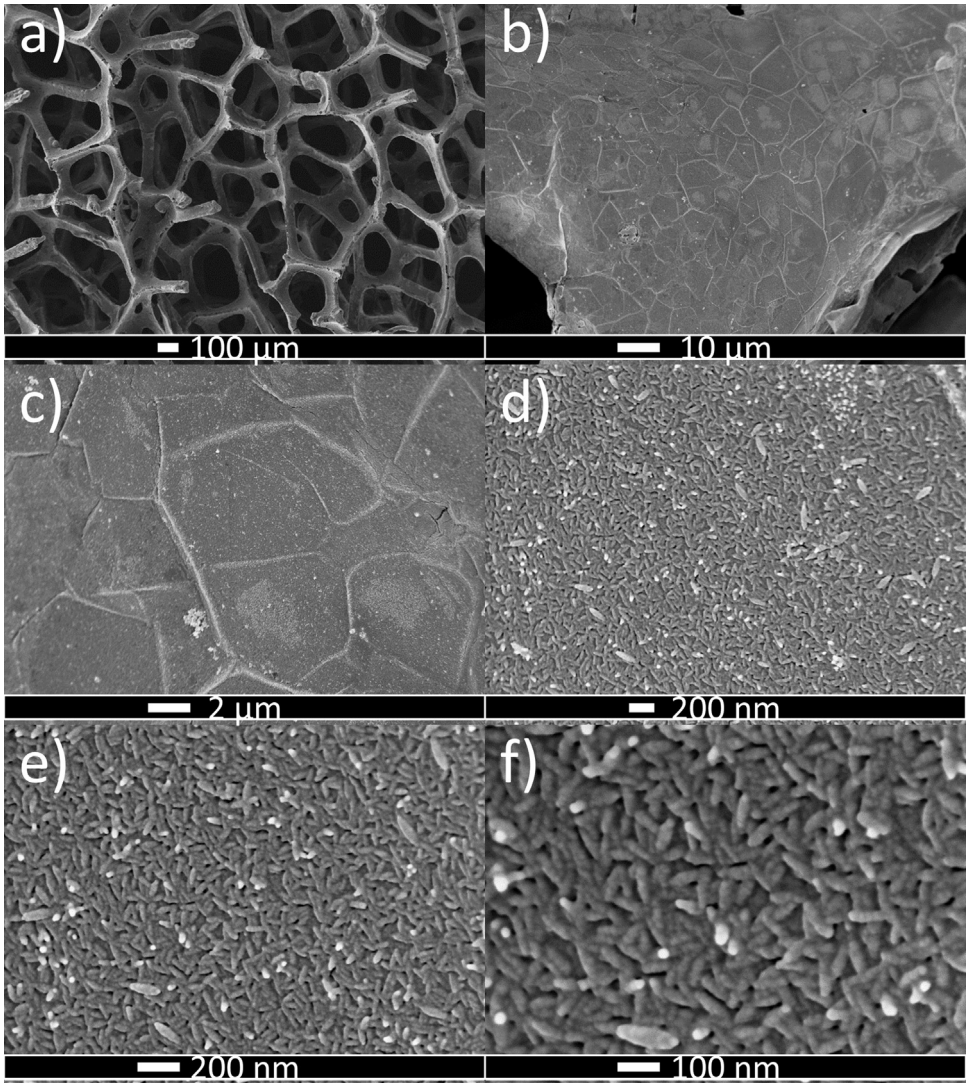

Fig. 2. FESEM images obtained at different magnification. (a) Microporous sponge-like network of 3D graphene; (b) Ligament-like interconnected network structure of 3D graphene; (c) wrinkled and rippled on 3D graphene; (d–f) Highly assembled Au nanorods assembled.

2879 (Fig. 3b). Thus, the resultant planes demonstrated that face-centered cubic of Au was obtained (Perumal et al., 2015a). The distinct changes in the diffraction peak corresponding to Au at 38.5° and 44.6° for (111) and (200) planes in tandem to the increasing Au thickness are clearly shown in Supplementary Fig. 4.

The Raman spectrum of synthesized 3D graphene before and after Au nanorods formation is shown in Fig. 4. The Raman spectrum for the CVD synthesized 3D graphene showcased its peak at 1589 cm^{-1} and

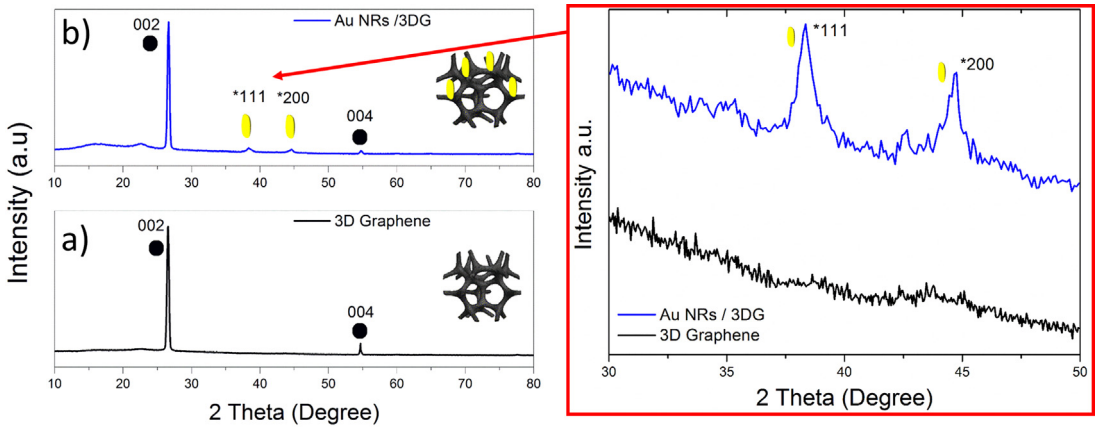

Fig. 3. XRD patterns of bare 3D graphene. (a) before and (b) after the formation of rod-like Au nanostructure. Insert shows the magnified XRD diffraction pattern of 3D Graphene/Au corresponding to (111) and (200) planes.

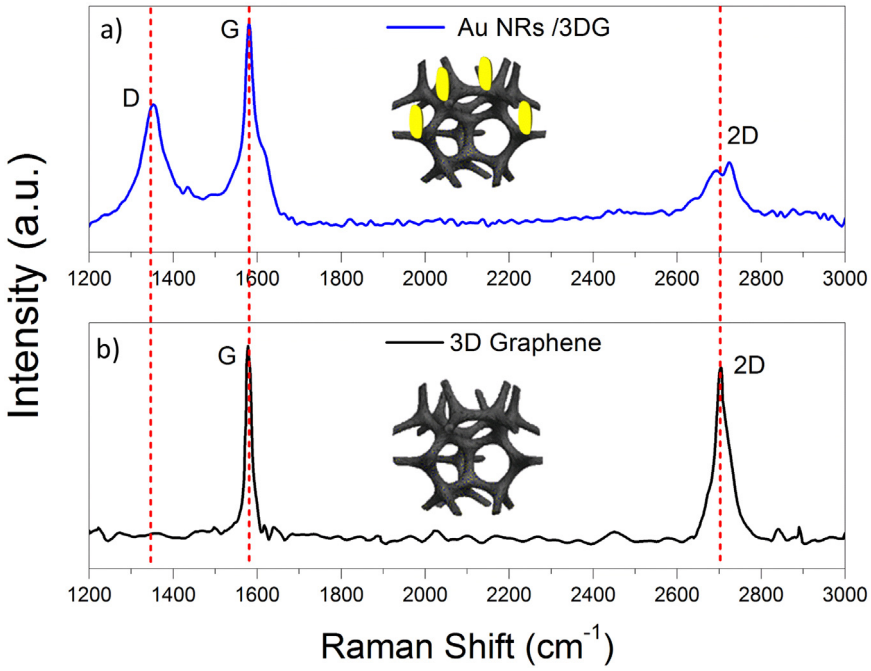

Fig. 4. Raman spectrum of synthesized 3D graphene (a) before and (b) after Au nanorods formation.

2710 cm^{-1} which corresponds to the G band and 2D band vibration mode of graphene for the normalised peaks obtained at 514 nm wavelength. The existence of the G band can be related to sp2 carbon atom vibration and the 2D band can be associated to the boundary phonon at Brillouin zone (Ferrari, 2007). There is no existence of defect-related peak corresponding to D band in the CVD synthesized 3D graphene, suggesting the production of high-quality 3D graphene (Beams et al., 2015). Having a defect-free graphene is crucial as it will ensure enhanced electrical properties of the fabricated material. Moreover, the 2D band and G band intensity, ratio and shape can be utilised to deduce the number of graphene layers synthesized (Ferrari, 2007; Mohiuddin et al., 2009). Interestingly, an additional peak is present at 1360 cm^{-1} corresponding to the D band appearing in the sample with 3D graphene and Au nanorods. The Raman spectrum of increasing Au thickness is shown in Supplementary Fig. 5. The rise of D peaks in the Au nanoparticle sample indicate the electron and hole recombination state on the 3D graphene surface. As the Au nanoparticle layer increases in thickness, the intensity of the D band peaks increases but there is no change in D band position. These phenomena indicate that higher electron and hole recombination occurs for thicker Au nanoparticles during the Raman laser-induced electron/hole scattering (Mohiuddin et al., 2009).

3.3. Impedimetric analysis of Mycobacterium tuberculosis

The Electrochemical Impedance Spectroscopy (EIS) has been employed to study the complex electrical resistance and interfacial properties of synthesized 3D graphene/Au nanorod (NR) composite biosensor. The biosensor were placed in 100 mM PBS solution (pH 7.4) containing 10 mM dissolved $[Fe(CN)6)]^{3-/4-}$ and frequency sweep was conducted in the range of 1–100 MHz for impedance measurement. Fig. 5a shows the Nyquist plot of Au NRs/3DG, pDNA/Au NRs/3DG and tDNA/pDNA/Au NRs/3DG electrode. The obtained Nyquist plot can be interpreted using a fitting model from Randles equivalent circuit (inset Fig. 5a). The fitting model comprises of bulk electrolyte resistance (Ra) with parallel combination of constant phase element (CPE), charge transfer resistance (Rct) and Warburg impedance related to diffusion of ions. The interaction between the interfacial layer of electrode and electrolyte solution (ferricyanide) is represented by the diameter of the semicircle with respect to the magnitude of charge transfer resistance. As shown in Fig. 5a and the insert (bar chart), the bare 3D graphene exhibits a high Rct value (~ 1.3 GΩ) compared to the modified 3D graphene with Au NRs (~ 37.3 MΩ). Such changes in the Rct value not only confirms the improvement over charge transfer properties but also reveals the synergistic effect between noble metal (Au) and 3D graphene (Low et al., 2017). In contrast, the Rct value for the probe DNA immobilized increases to ~ 316.1 MΩ, which can be attributed to the hindrance of ferricyanide anion at the electrode surface due to the electrostatic repulsion of negatively charged phosphoric acid from the immobilized ssDNA. Self-assembly monolayer by using Au-SH bonding directly on Au nanorods surface which lead to higher loading of DNA which significantly block the diffusion of ions onto the electrode interface. The Au nanorods-radii in combination with the increased surface area due to irregularly spaced structure with rippled surfaces of 3D graphene, significantly enhances the SAM efficiency lead to increased immobilization rates and enhanced hybridization efficiency. Further increment in the Rct value (862.3 MΩ) is observed for the target hybridized electrode (tDNA/Au NRs/3D). The obtained results suggests successful immobilization and hybridization of DNA on the prepared bio-electrode (Hu et al., 2011). Similar increase in the EIS induced by the relatively larger biomolecule complexes formation on electrode surface has been proven by several recent studies in the literature, including Au/MCH/ssDNA/dsDNA, IDE/ZnO-Au NPs/Antigen/Antibody and C1–P1/Au NPs/TB–GO/GCE (Gopinath et al., 2016; Matsishin et al., 2015; Peng et al., 2015). Fig. 5b shows the impedimetric semicircle response of pDNA/Au NRs/3DG bio-electrode hybridized with different concentrations of complementary target DNA (i–viii) 10 fM to 0.1 μM. Substantially, the value of charge transfer resistance increases upon increasing the concentration of complementary target DNA due to significant rise in electrostatic repulsion force between anions and the negatively charged tDNA molecule. Thus, the resultant Rct confirms the successful detection of various linear range (10 fM to 0.1 μM) of tDNA on 3D graphene/Au NRs bio-electrode exemplifying the superiority of purpose sensing elements. The excellent bio-sensing mechanism of the 3D graphene/Au NRs are due to the fact that 3D graphene has a large active surface area that could provide a platform for high catalytic activity (Loan et al., 2018). Moreover, adherence of Au nanoparticles on the irregular and rippled surfaces of 3D graphene leads to the

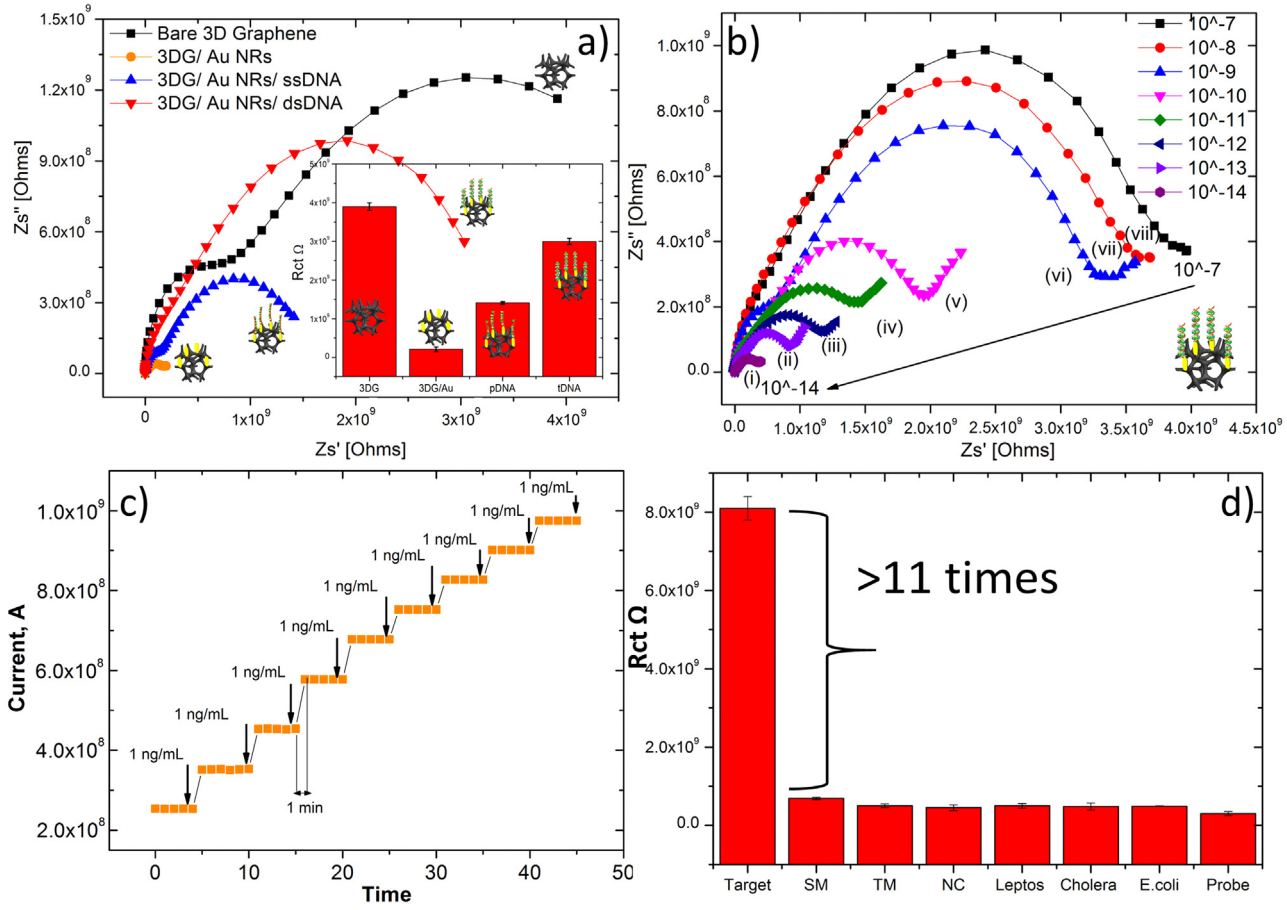

Fig. 5. (a) Impedance spectra of (a) Au-nanorod embedded 3D graphene with p-DNA immobilization and t-DNA hybridization. The figure inset displays the changes in Rct with 3D graphene before and after Au nanorod formation. (b) Impedimetric response curve of Au-nanorod embedded 3D graphene nanocomposite/p-DNA hybridized with different concentrations of complementary target DNA (i–viii) 10 fM to 0.1 μM. (c) Shows the electroanalytical curve for 1 min response time. (d) Specificity analysis on Au-nanorod embedded 3D graphene.

formation of Au nanorods which further increases the electrocatalytic capability of the composite. Furthermore, the introduction of Au nanorods has also provided an alternate method for biomolecule immobilization without the need of chemical exfoliation of graphene structures which could lead to poor electrical conductivity. Finally, the coupling of noble metal (Au) and 3D graphene accelerates the charge transfer properties which confer unparalleled electrochemical performance.

3.4. High analytical performance of 3D graphene/Au nanorods composite

The electroanalytical response of Au nanorod on 3D graphene shown in Fig. 5c showcases real-time detection of the proposed DNA sensor along with the complementary DNA concentrations. For each injection of 1 nM of DNA target, five measurements were consecutively taken for 5 min to exhibit the continuity of the DNA sensor. Upon injection of the complementary DNA, the current response increased rapidly and reached a high 95–97% of the steady state current within 1 min, indicating level saturation. These results suggest that the response time for this DNA sensor can be 1 min with the complete duplex formation. The detection limit of 10 femtomolar was estimated for the purpose biosensor using signal to noise ratio as more than 3σ. In order to determine the specificity of the purpose biosensor, different DNA strands including non-complementary, single-base mismatch DNAs and three-base mismatches DNA were tested by passing them independently on probe DNA immobilized electrode (Fig. 5d). In addition to that, cross specificity with other bacteria DNA strands such as Leptospira sp., *Escherichia coli* and *Vibrio cholera* were evaluated. The charge transfer resistance value of single mismatched DNA strands was found to be ~ 687.2 MΩ compared to 8.1 GΩ Rct value of the target DNA (1 nM). Similarly, the Rct of cross-specificity for Leptospira sp., *E. coli* and *V. cholera* are 501.7 MΩ, 491.4 MΩ and 482.3 MΩ, respectively. The current analytical system displays 12-fold higher detection of target DNA compared to the single mismatched DNA and other strands with the same concentration which indicates that the proposed DNA biosensor has excellent sequence specificity. In comparison to previously reported literature, these results obtained are the highest and thus demonstrates the best sensitivity and specificity (Hu et al., 2011; Loan et al., 2018; Low et al., 2017). Further, the comparison of analytical performance with different DNA sensor shown in Supplementary Table S1 (Diouani et al., 2008; Hajihosseini et al., 2016; Mat Zaid et al., 2017).

4. Conclusion

A new nanocomposite for biosensing application was shown in this study with the appealing characteristics of high conductivity and sensitivity, large active surface area, defect-free structure and excellent electrical properties. The capability of the nanocomposite with Au nanorods embedded on 3D graphene as an excellent transducer has been lucidly demonstrated. Au nanorod like nanostructure was fabricated potentially due to the irregularly spaced structure and rippled morphology of 3D graphene. The progression of this Au nanostructure from nanoparticle to rod-like appearance was clearly displayed by morphological observations and supported concretely by structural analyses.

This unique nanocomposite was further utilised for impedimetric analysis to detect the specific DNA sequences responsible for tuberculosis. The reported biosensor satisfactorily attained femtomolar level of sensitivity with excellent specificity. This high performance might be attributed to the proper spatial arrangement that was brought about by the embedded Au nanorod and the well-aligned immobilised probe DNA sequence. In addition to that, the surface is greatly expanded owing to the formation of Au nanorods. However, this strategy may limit the rippled texture on 3D graphene available in this study and probably other metallic thin films may produce different ripple structures. Future developments with graphene can have similar directions as elucidated in the present study in order to successfully implement the proposed strategy to diagnose other disease biomarkers. The creation of suitable surface chemistry to immobilize or capture other biomolecules such as protein, aptamer, glycans on the graphene, will aid the diagnosis of various chronic and infectious diseases as well as strengthen pathogenic surveillance. The novel composite mediated device demonstrated here is highly feasible and has pitched a plethora of ideas towards the future biosensors development and opened new directions for nano-diagnostic systems.

Acknowledgements

The authors are indebted to Universiti Teknologi Petronas (UTP) for the opportunity given to conduct the research in the Nanotechnology Research Laboratory and Dye Solar Cell Laboratory. We would also like to convey our thanks to Universiti Malaysia Perlis (UniMAP) for providing the research facilities in the Nano Biochip Laboratory. The appreciation goes to all team members and staffs in the Centre of Innovative Nanostructures and Nanodevices (COINN).

Competing interests

The authors declare no competing financial interests. All authors have approved the final manuscript for submission.

Appendix A. Supplementary material

Supplementary data associated with this article can be found in the online version at http://dx.doi.org/10.1016/j.bios.2018.05.042.

References

Al-ani, L.A., Alsaadi, M.A., Kadir, F.A., Hashim, N.M., Julkapli, N.M., Yehye, W.A., 2017. Graphene-gold based nanocomposites applications in cancer diseases; Efficient detection and therapeutic tools. Eur. J. Med. Chem. 139, 349–366. http://dx.doi.org/10.1016/j.ejmech.2017.07.036.

Beams, R., Gustavo Cançado, L., Novotny, L., 2015. Raman characterization of defects and dopants in graphene. J. Phys. Condens. Matter 27. http://dx.doi.org/10.1088/0953-8984/27/8/083002.

Chen, Z., Ren, W., Gao, L., Liu, B., Pei, S., Cheng, H.M., 2011. Three-dimensional flexible and conductive interconnected graphene networks grown by chemical vapour deposition. Nat. Mater. 10, 424–428. http://dx.doi.org/10.1038/nmat3001.

Diouani, M.F., Helali, S., Hafaid, I., Hassen, W.M., Snoussi, M.A., Ghram, A., Jaffrezic-Renault, N., Abdelghani, A., 2008. Miniaturized biosensor for avian influenza virus detection. Mater. Sci. Eng. C Mater. Biol. Appl. 28, 580–583. http://dx.doi.org/10.1016/j.msec.2007.10.043.

Fang, Q., Shen, Y., Chen, B., 2015. Synthesis, decoration and properties of three-dimensional graphene-based macrostructures: a review. Chem. Eng. J. 264, 753–771. http://dx.doi.org/10.1016/j.cej.2014.12.001.

Ferrari, A.C., 2007. Raman spectroscopy of graphene and graphite: disorder, electron-phonon coupling, doping and nonadiabatic effects. Solid State Commun. 143, 47–57. http://dx.doi.org/10.1016/j.ssc.2007.03.052.

Gao, H., Duan, H., 2015. 2D and 3D graphene materials: preparation and bioelectrochemical applications. Biosens. Bioelectron. 65, 404–419. http://dx.doi.org/10.1016/j.bios.2014.10.067.

Georgakilas, V., Otyepka, M., Bourlinos, A.B., Chandra, V., Kim, N., Kemp, K.C., Hobza, P., Zboril, R., Kim, K.S., 2012. Functionalization of graphene: covalent and non-covalent approaches, derivatives and applications. Chem. Rev. 112, 6156–6214. http://dx.doi.org/10.1021/cr3000412.

Global Tuberculosis Report, 2017. Global Tuberculosis Programme, & World Health Organization. ⟨https://doi.org/WHO/HTM/TB/2017.23⟩.

Gopinath, S.C.B., Perumal, V., Kumaresan, R., Lakshmipriya, T., Rajintraprasad, H., Rao, B.S., Arshad, M.K.M., Chen, Y., Kotani, N., Hashim, U., 2016. Nanogapped impedimetric immunosensor for the detection of 16 kDa heat shock protein against Mycobacterium tuberculosis. Microchim. Acta 183, 2697–2703. http://dx.doi.org/10.1007/s00604-016-1911-7.

Hajihosseini, S., Nasirizadeh, N., Hejazi, M.S., Yaghmaei, P., 2016. A sensitive DNA biosensor fabricated from gold nanoparticles and graphene oxide on a glassy carbon electrode. Mater. Sci. Eng. C 61, 506–515. http://dx.doi.org/10.1016/j.msec.2015.12.091.

Hu, Y., Hua, S., Li, F., Jiang, Y., Bai, X., Li, D., Niu, L., 2011. Green-synthesized gold nanoparticles decorated graphene sheets for label-free electrochemical impedance DNA hybridization biosensing. Biosens. Bioelectron. 26, 4355–4361. http://dx.doi.org/10.1016/j.bios.2011.04.037.

Loan, P.T.K., Wu, D., Ye, C., Li, X., Tra, V.T., Wei, Q., Fu, L., Yu, A., Li, L.J., Lin, C. Te, 2018. Hall effect biosensors with ultraclean graphene film for improved sensitivity of label-free DNA detection. Biosens. Bioelectron. 99, 85–91. http://dx.doi.org/10.1016/j.bios.2017.07.045.

Low, S.S., Loh, H.S., Boey, J.S., Khiew, P.S., Chiu, W.S., Tan, M.T.T., 2017. Sensitivity enhancement of graphene/zinc oxide nanocomposite-based electrochemical impedance genosensor for single stranded RNA detection. Biosens. Bioelectron. 94, 365–373. http://dx.doi.org/10.1016/j.bios.2017.02.038.

Mat Zaid, M.H., Abdullah, J., Yusof, N.A., Sulaiman, Y., Wasoh, H., Md Noh, M.F., Issa, R., 2017. PNA biosensor based on reduced graphene oxide/water soluble quantum dots for the detection of Mycobacterium tuberculosis. Sens. Actuators B Chem. 241, 1024–1034. http://dx.doi.org/10.1016/j.snb.2016.10.045.

Matsishin, M., Rachkov, A., Errachid, A., Dzyadevych, S., Soldatkin, A., 2015. Development of impedimetric DNA biosensor for selective detection and discrimination of oligonucleotide sequences of the rpoB gene of Mycobacterium tuberculosis. Sens. Actuators B Chem. 222, 1152–1158. http://dx.doi.org/10.1016/j.snb.2015.08.012.

Mohiuddin, T.M.G., Lombardo, A., Nair, R.R., Bonetti, A., Savini, G., Jalil, R., Bonini, N., Basko, D.M., Galiotis, C., Marzari, N., Novoselov, K.S., Geim, A.K., Ferrari, A.C., 2009. Uniaxial strain in graphene by Raman spectroscopy: G peak splitting, Grüneisen parameters, and sample orientation. Phys. Rev. B – Condens. Matter Mater. Phys. 79, 1–8. http://dx.doi.org/10.1103/PhysRevB.79.205433.

Peng, H.P., Hu, Y., Liu, P., Deng, Y.N., Wang, P., Chen, W., Liu, A.L., Chen, Y.Z., Lin, X.H., 2015. Label-free electrochemical DNA biosensor for rapid detection of multidrug resistance gene based on Au nanoparticles/toluidine blue-graphene oxide nanocomposites. Sens. Actuators B Chem. 207, 269–276. http://dx.doi.org/10.1016/j.snb.2014.10.059.

Perumal, V., Hashim, U., Gopinath, S.C.B., Haarindraprasad, R., Foo, K.L., Balakrishnan, S.R., Poopalan, P., 2015a. "Spotted nanoflowers": gold-seeded zinc oxide nanohybrid for selective bio-capture. Sci. Rep. 5, 12231. http://dx.doi.org/10.1038/srep12231.

Perumal, V., Hashim, U., Gopinath, S.C.B., Haarindraprasad, R., Poopalan, P., Liu, W.-W., Ravichandran, M., Balakrishnan, S.R., Ruslinda, A.R., 2015b. A new nano-worm structure from gold-nanoparticle mediated random curving of zinc oxide nanorods. Biosens. Bioelectron. 78, 14–22. http://dx.doi.org/10.1016/j.bios.2015.10.083.

Qiu, H.J., Guan, Y., Luo, P., Wang, Y., 2017. Recent advance in fabricating monolithic 3D porous graphene and their applications in biosensing and biofuel cells. Biosens. Bioelectron. 89, 85–95. http://dx.doi.org/10.1016/j.bios.2015.12.029.

Saheed, M.S.M., Mohamed, N.M., Singh, B.S.M., Saheed, M.S.M., 2017. Precursor and pressure dependent 3D graphene: a study on layer formation and type of carbon material. Diam. Relat. Mater. 79, 93–101. http://dx.doi.org/10.1016/j.diamond.2017.09.004.

Sahoo, P.K., Aepuru, R., Panda, H.S., Bahadur, D., 2015. Ice-templated synthesis of multifunctional three dimensional graphene/noble metal nanocomposites and their mechanical, electrical, catalytic, and electromagnetic shielding properties. Sci. Rep. 5, 1–12. http://dx.doi.org/10.1038/srep17726.

Shi, L., Wang, Y., Ding, S., Chu, Z., Yin, Y., Jiang, D., Luo, J., Jin, W., 2017. A facile and green strategy for preparing newly-designed 3D graphene/gold film and its application in highly efficient electrochemical mercury assay. Biosens. Bioelectron. 89, 871–879. http://dx.doi.org/10.1016/j.bios.2016.09.104.

Shojaei, T.R., Mohd Salleh, M.A., Tabatabaei, M., Ekrami, A., Motallebi, R., Rahmani-Cherati, T., Hajalilou, A., Jorfi, R., 2014. Development of sandwich-form biosensor to detect Mycobacterium tuberculosis complex in clinical sputum specimens. Braz. J. Infect. Dis. 18, 600–608. http://dx.doi.org/10.1016/j.bjid.2014.05.015.

Srivastava, S.K., van Rijn, C.J.M., Jongsma, M.A., 2016. Biosensor-based detection of tuberculosis. RSC Adv. 6, 17759–17771. http://dx.doi.org/10.1039/C5RA15269K.

Sundaram, R.S., Steiner, M., Chiu, H.Y., Engel, M., Bol, A.A., Krupke, R., Burghard, M., Kern, K., Avouris, P., 2011. The graphene-gold interface and its implications for nanoelectronics. Nano Lett. 11, 3833–3837. http://dx.doi.org/10.1021/nl201907u.

Xiao, X., Beechem, T.E., Brumbach, M.T., Lambert, T.N., Davis, D.J., Michael, J.R., Washburn, C.M., Wang, J., Brozik, S.M., Wheeler, D.R., Burckel, D.B., Polsky, R., 2012. Lithographically defined three-dimensional graphene structures. ACS Nano 6, 3573–3579. http://dx.doi.org/10.1021/nn300655c.

Yan, H., Zhang, H., Huang, S., Yu, X., Gao, X., Chang, J., 2017. Biosensors and bioelectronics synthesis of ZnO nanowire arrays/3D graphene foam and application for determination of levodopa in the presence of uric acid. Biosens. Bioelectron. 89, 592–597. http://dx.doi.org/10.1016/j.bios.2016.01.078.